All-dielectric metasurface absorbers for uncooled terahertz imaging: supplementary material

KEBIN FAN[1], JONATHAN Y. SUEN[1], XINYU LIU[1], AND WILLIE J. PADILLA[*]

[1] Department of Electrical and Computer Engineering, Duke University, Box 90291, Durham, NC 27708, USA
[*] Corresponding author: willie.padilla@duke.edu

Published 31 May 2017

This document provides supplementary information to "All-dielectric metasurface absorbers for uncooled terahertz imaging," https://doi.org/10.1364/optica.4.000601. We provide details on our experimental methods and derivation of the absorber performance. © 2017 Optical Society of America

https://doi.org/10.1364/optica.4.000601.s001

1. THE MINIMUM RADIUS OF DIELECTRIC METAMATERIAL ABSORBERS

The theory of the dielectric metamaterial absorber has been presented previously.[1] Here we detail derivation of the minimum radius of the dielectric metamaterial absorber. We require that for the cutoff condition of the hybrid electric mode, the fields should be confined inside the dielectric cylinders as shown in Fig. S1. This requirement is analogous to the geometrical optics condition where the angle of incidence on the sidewalls equals the critical angle for total internal reflection. [2] We consider a general wavevector inside our guide (k_g) and break it into two components in the radial and axial directions, i.e. $k_g = k_r + k_z$. Thus the critical angle θ_c for total internal reflection inside a dielectric waveguide is given by,

$$\cos\theta_c = \frac{k_r}{k_g} \tag{S1}$$

The guide wavector is given in terms of the wavelength inside the material as $k_g = 2\pi/\lambda_g$, where $\lambda_g = \lambda_0/n_g = \lambda_0/\sqrt{\epsilon_r}$. Here n_g, ϵ_r is the guide index and relative dielectric function, respectively. Snell's law for total internal reflection inside the guide is $\sin^2(\theta_c) = n_g^{-2}$ and plugging into Eq. S1 and solving for the radial wavevector we find,

$$k_r = k_g\sqrt{1-\frac{1}{n_g^2}} = \frac{2\pi}{\lambda_g}\sqrt{1-\frac{1}{n_g^2}} \tag{S2}$$

In addition, the wavevector k_r at the cutoff condition is determined by roots of the Bessel function of the first kind, i.e., $J_1(k_r r) = 0$. For the supported lowest order EH mode at the absorption resonance the minimum radius is thus determined by,

$$r = \frac{3.83}{k_r} = 3.83\frac{\lambda_g}{2\pi}(1-n_g^{-2})^{-1/2} \tag{S3}$$

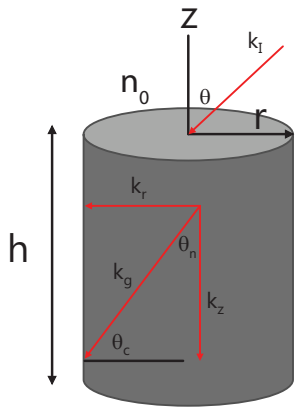

Fig. S1. Schematic view of a dielectric cylinder with radius of r and height of h. k_g, k_r, K_z are the wavevectors for the guide wave, radial propagation, and longitudinal propagation, respectively. θ_c is the critical angle for the total internal reflection, and θ_n is the complement angle of θ_c.

Simplifying and plugging in for the free space wavelength we find,

$$r = 0.61\frac{\lambda_0}{\sqrt{n_g^2-1}} \tag{S4}$$

The minimum height of the dielectric cylinder is given by the condition for a half-wave dipole, i.e.,

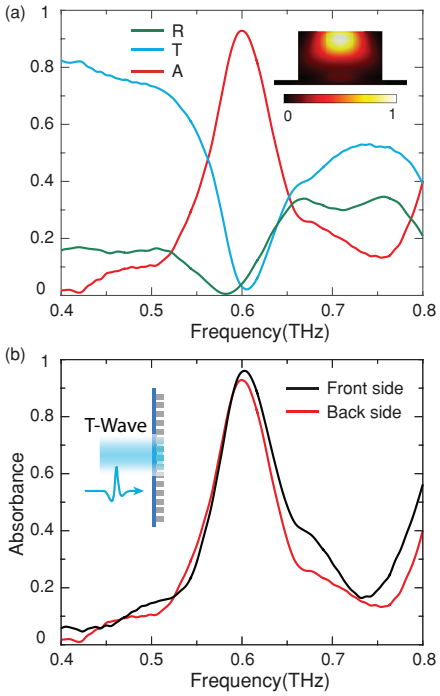

Fig. S2. (a) Measured reflectance (green), transmittance (blue), and absorbance (red) of the absorber. The inset shows the cross-section (x-z plane) view of the power loss density distribution. The wave is polarized in the x direction. (b) Comparison of the absorbances between the terahertz incidence from the front side (black) and back side (red), respectively. The inset illustrates the incidence from the back side of the absorber.

$$h = \frac{\lambda_0}{2n_g} \tag{S5}$$

Given a material with an index (n), one may use Eqs. (S4) and (S5) to determine the height and radius of an all-dielectric metasurface absorber.

Interestingly if, instead of using Eq (S2), we relate the critical angle in Eq. (S1) to the angle of incident radiation (θ) external to the cylinder, as shown in Fig. S1, we find the minimum cylinder radius is given by,

$$r = 0.61\frac{\lambda_0}{n_g \sin\theta_n} = 0.61\frac{\lambda_0}{n_0 \sin\theta}. \tag{S6}$$

where n_0 is the refractive index of medium outside the cylinder. Equation S6 corresponds the Rayleigh criterion for the diffraction limit by circular apertures. [3] Thus although we arrived at Eqs. (S4) and (S6) through an argument based on total internal reflection, we find that our condition for absorption is identical to that of the diffraction limit.

2. THZ-TDS MEASUREMENT OF THE ABSORBER

Figure 1a shows experimental results with the terahertz wave incident from the back side of the metasurface (PDMS substrate side). The measured peak absorbance at 600 GHz is over 90%, close to that with incidence from the front side. The small difference between these two absorbances as shown in Fig. S2b can be attributed to the PDMS substrate-induced asymmetry.

3. INFRARED MEASUREMENTS OF MATERIALS

Through FTIR spectrometer measurements, we also characterized the scattering properties of various materials used in our imaging experiments, i.e. PDMS and black polyethylene. Figure S3a shows the measured absorbance (red) or, equivalently, the emissivity of the 8-μm thick PDMS thin film and shows that it is over 0.9 from 8 to 10 μm, which covers the range where the blackbody radiation peaks around 300 K. Figure S3b shows the measured transmittance of a 75-μm thick black polyethylene film, which only allows 25% of power transmitted from 8 to 10 μm. For our imaging experiment, therefore, the total thermal radiation from source to the IR camera in the 8 - 10 μm band is significantly attenuated, as shown in the red curve shown in Fig. S3b.

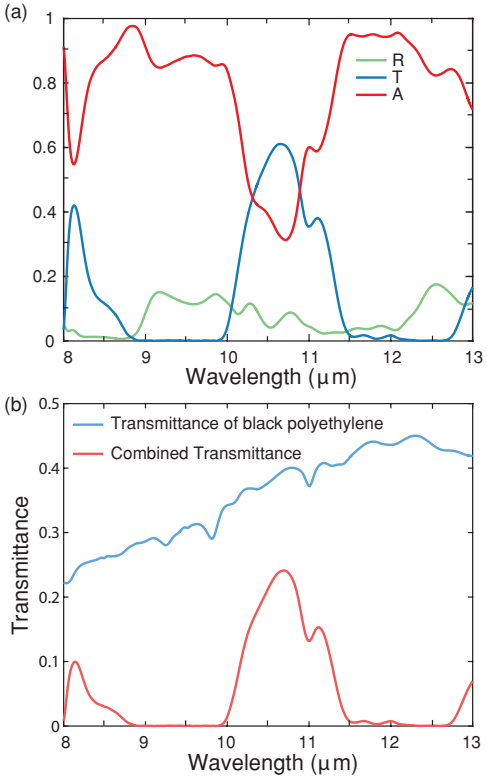

Fig. S3. (a) Measured reflectance (green), transmittance (blue), and absorbance (red) of the 8-μm PDMS thin film in the long-wave infrared region (8 - 13 μm). (b) Blue curve shows measured transmittance of the 75-μm black polyethylene in the infrared range. Red curve shows the total infrared transmittance through the black polyethylene and 8-μm PDMS thin film to the IR camera.

4. THZ POWER ON THE ABSORBER AND IMAGING DIFFRACTION LIMIT

In this section, we first estimate the responsivity of the absorber with a focused terahertz beam. The synthesized terahertz wave emits from a diagonal horn, which was placed at the focus point of the parabolic mirror OAP1 with an effective focal length of f_{OAP1} = 190.6 mm and diameter of D_{OAP1} = 50.8 mm. According to the diagonal horn specification, the beam is approximated to be a Gaussian beam with a full 3-dB beamwidth of 10 degrees. Then the estimated full 3-dB beam size at the mirror OAP1 is

about

$$d_{OAP1} = 2f_{OPA1}\tan(\theta_{3dB}/2) = 33.3\ \text{mm}. \quad \textbf{(S7)}$$

Because of the limited diameter of the mirror OAP1, the quasi-collimated beam is truncated with a truncation factor of $\alpha_T = d_{OAP1}/\sqrt{\ln 2/2}/D_{OAP1} = 1.1$. As a result, the portion of reflected power is about $\eta_P = 1 - \exp\{-2/\alpha_T^2\} = 0.8$. Then the terahertz beam was focused again via the second parabolic mirror OAP2, with both the effective focal length and diameter of 50.8 mm and averaged numerical aperture NA of 0.49. Given the truncation, the focused beam profile is a hybrid between an Airy and a Gaussian pattern. For the sake of simplificity, we still use the Gaussian beam to estimate the power incident on the absorber. Then the radius of the beam at the $1/e^2$ of intensity on the focal point can be estimated by [4]

$$s_{E2} = 0.5K_{E2}\lambda/(NA) = 0.9\ \text{mm}, \quad \textbf{(S8)}$$

where K_{E2} is a spot size constant that is a function of the truncation factor, equal to 1.78 at $1/e^2$ intensity. On the other hand, the atmospheric attenuation on the 600 GHz is about 0.2 dB/m [5], which can be ignored. The diagonal antenna coupling efficiency is about η_{ac} =84.3% [6]. Additionally, a 75-μm thick film of black polyethylene was placed in the optics; the transmittance of the film at terahertz frequencies is about η_{bp} = 80% [7]. Combining the above, the toal power incident on the absorber is approximately

$$\begin{aligned} P_{ta} &= \eta_{ac}\eta_P\eta_{bp}\eta_{abs}P_{inc} \\ &= 0.843 \times 0.8 \times 0.8 \times 0.959 \times 2.1\ \text{mW} \\ &= 1.09\ \text{mW}, \end{aligned} \quad \textbf{(S9)}$$

where the incident power P_{inc} at 605 GHz is about 2.1 mW and the absorption η_{abs} is 0.959 at 605 GHz measured from experiments. Accordingly, the power incident on the central pixel is about 250 μW. Finally, the responsivity is about $R = \Delta T/P_{uc} = 2.16 \times 10^4$ K/W.

In the imaging experiment, the magnification of the imaging system is about 0.11, which is estimated from thin lens formula. Given the numerical aperture of OAP2 is about 0.49, the Rayleigh diffraction limited beam size can be estimated to be [3]

$$d_{lim} = 0.61\lambda/NA = 620\ \mu\text{m} \quad \textbf{(S10)}$$

which is a little larger than the projected image feature size of 565 μm. Therefore, our imaging quality is limited by diffraction. This diffraction is also confirmed by our geometric optics simulation. Through further optimization on imaging system and integration with an IR camera, we believe much better images can be obtained through a highly responsive metasurface absorber, for example, sealing the absorber in a vacuum environment to limit the thermal loss from convection, which will be explained in the next section.

5. COUPLED ELECTROMAGNETIC-THERMAL ANALYSIS

We modeled the heat transfer of the metasurface absorber through conduction, radiation, and convection both with an analytic estimation and by a multiphysics numerical simulation, which coupled terahertz energy absorption with a thermal model. Convection causes the majority of heat transfer, which is also confirmed by our numerical simulations, where in-plane boundaries were set as open and floating temperature with the room temperature of 293 K. For these simulations, the incident power on the array was calculated from the Gaussian beam assumption in last section. Simulations were also performed to compare temperature increases with and without the convection processes or radiation while other heat transfer processes were retained. As shown in Fig. S4, the stable temperature at the center of the array without convection increases from 293 K to about 297.7 K, which is about 1.7 K higher than that with all processes considered. However, when excluding the radiation process only, the steady-state temperature increase is about 0.25 K higher. As a result, the temperature drop due to convection is about 6.76 times higher than the temperature drop from radiation. This value is very close to the ratio of the convective conductance to the radiative conductance.

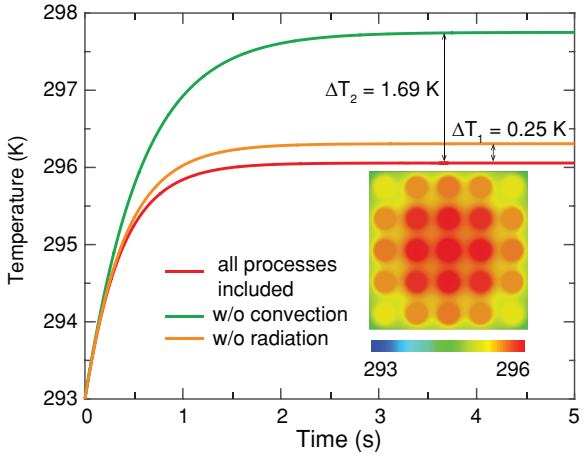

Fig. S4. Numerical simulation of the temperature distribution over the 5 × 5 cylinder arrays with a plane wave incidence. For comparison, the transient temperature changes ignoring convection and radiation respectively are also shown. The inset presents the stable temperature distribution over the array with all thermal processes included. In our numerical simulations, open boundaries with a floating temperature were used.

Equation S11 shows steady-state thermal transport in the absorber with all the three processes – thermal conduction, natural convection and radiation, included. For the transient state with a time-varying signal, the thermal mass of the structures has to be taken into account,

$$\epsilon_m P_i + P_a(T_a) = P_{loss} + C\frac{dT}{dt}, \quad \textbf{(S11)}$$

where ϵ_m is the absorbance of the metasurface at terahertz frequencies, $P_i = P_0 + P_m e^{i\omega t}$ is the incident terahertz power including steady part P_0 and a time varying part P_m with modulation frequency of ω, $P_{loss} = G_T(T - T_a)$ is the total loss through conduction, convection and radiation, given by $G_T = G_{cond} + G_{conv} + G_{rad}$. P_{cond} is the power loss through conductive thermal transfer mainly in the supporting substrate, P_{conv} is the power loss due to the free thermal convection to the air, P_{rad} is the power loss from the infrared radiation of the heated cylinders and substrate, $T = T_0 + \Delta T e^{i\omega t}$ is the temperature on the bolometer induced by the input power with steady part and time varying part, and $P_a = \sigma\epsilon_m\epsilon_{air}AT_a^4$ is the absorbed power from the surrounding air. σ is the Stefan-Boltzmann constant, A is the emission area and ϵ_m is the absorptivity of the materials, including PDMS substrate and silicon, ϵ_{air} is the emissivity of the air, and C is the thermal conductance of the whole

structure. Equating the time varying terms yields

$$\Delta T = \frac{\epsilon_m P_m}{\sqrt{G_T^2 + \omega^2 C^2}}. \quad \textbf{(S12)}$$

The the net radiated power is,

$$P_{rad} = \sigma \epsilon A (T^4 - T_a^4) \quad \textbf{(S13)}$$

We expand the term in parenthesis which yields,

$$P_{rad} = \sigma \epsilon A \left[4T_a^3 \Delta T \left(1 + \frac{\Delta T}{T_a} + \frac{3}{4}\left(\frac{\Delta T}{T_a}\right)^2 + \frac{1}{4}\left(\frac{\Delta T}{T_a}\right)^3 \right) \right] \quad \textbf{(S14)}$$

where the temperature change $\Delta T = T - T_a$ is very small compared to the room temperature. We thus keep only leading-order ΔT terms, thus giving the radiated power as,

$$P_{rad} \approx 4\sigma \epsilon A T_a^3 \Delta T = G_{rad} \Delta T \quad \textbf{(S15)}$$

Consequently, the temperature increase on the metasurface due to the incident terahertz wave can be written as,

$$\Delta T \approx \frac{\epsilon_m P_m}{\sqrt{(G_{cond} + G_{conv} + G_{rad})^2 + \omega^2 C^2}} \quad \textbf{(S16)}$$

Since the temperature distribution over the metasurface is very complicated, it is onerous to calculate the heat flux from each process accurately. However, to evaluate the contributions of these three processes, it is possible to roughly estimate them by assuming the incident power is focused on the center of a 5×5 cylinder array. From Fig. 2 and Fig. 3b, the temperature increases mostly in the center of a 3×3 array, thus the boundaries of this finite array can be approximated as the room temperature at 293 K. In the conduction process, heat is mainly drained through the PDMS substrate. Neglecting the thermal conduction process from the heated silicon cylinder to PDMS, the thermal conductance spreading from the center to boundaries can be estimated to be

$$\begin{aligned} G_{cond} &= k_{pdms} 2\pi t_{pdms} / \ln(r_2/r_1) \\ &= 3.67 \times 10^{-6}\ \mathrm{W/K}, \end{aligned} \quad \textbf{(S17)}$$

where $k_{pdms} = 0.15$ W/m/K, t_{pdms} is the thickness of the PDMS thin film, r_2 is the outer radius of the center 5×5 cylinder array, and $r_1 = 0.106$ mm is the radius of the thermal transport from the center with a presumption that the center cylinder is uniformly heated.

The thermal convective process takes place between several interfaces, particularly the silicon to air, the front side of PDMS to air and the backside of PDMS to air. The thermal convective coefficient for a vertically positioned structure with temperature T from the room temperature T_a can be estimated to be [8]

$$\begin{aligned} h_{conv} &= \frac{k_{air}}{L} Nu \\ &= \frac{k_{air}}{L} \left\{ 0.68 + \frac{0.67 Ra^{1/4}}{[1 + (0.492/Pr)^{9/16}]^{4/9}} \right\}, \end{aligned} \quad \textbf{(S18)}$$

where L is the characteristic length of the heated area with L_{pdms} = 1.65 mm for PDMS thin film and averaged L_{si} = 1.06 mm for silicon cylinders, Nu is the Nusselt number, Ra is the Rayleigh number and Pr is the Prandtl number, both of air [8]. Considering a small temperature change barely affects the convective coefficient, we estimated $h_{PDMS} = 20$ W/m^2 K and $h_{Si} = 32$ W/m^2 K by assuming average temperature increase up to 5 K above room temperature. Accordingly, the conductance due to the thermal convection is estimated to be $G_{conv} = h_{pdms} \times A_{pdms} + h_{Si} \times A_{Si} \approx 1.22 \times 10^{-4}$ W/K. This conductance is underestimated since we ignored the convection from side walls for simplicity.

For the thermal radiation, on account of the negligible infrared emissivity of lightly doped silicon (from the Drude model), we only consider the thermal radiation from the front and back faces of the PDMS thin film, based on our experimental results shown in Fig. 2. Then the net thermal radiation relative to temperature change can be given by

$$G_{rad} = \sigma \bar{\epsilon}_{pdms} A \iint \frac{T(x,y)^4 - T_a^4}{T(x,y) - T_a} dxdy \quad \textbf{(S19)}$$

where $\bar{\epsilon}_{pdms}$ is the emissivity of PDMS, which is about 0.8 in the range of 8 - 10 μm. $T(x,y)$ and T_a both are obtained from experimental results shown in Fig. 2. Then the radiative conductance from the backside of PDMS can be easily calculated from experiments to be about 1.5×10^{-5} W/K. For the front side of PDMS film, we have to exclude the area patterned with less emissive silicon cylinders. Since the temperature difference between the silicon area and PDMS area is small, the radiative conductance is nearly proportional to the area only. Then, we have the total G_{rad} about 2.5×10^{-5} W/K. The thermal capacitance can be easily calculated based on the material properties and the volume of the PDMS thin film and silicon cylinders in the center array, which was found to be about about 5.5×10^{-5} J/K. We have to point out that this capacitance is overestimated with an assumption of the uniform temperature distribution over the modeled metasurface array rather than a strongly localized thermal distribution in our experiment. As a result, the analytically calculated ΔT for a modulated input at 0.25 Hz is about 6.25 K, which is a little higher than the experiment result shown in Fig. 2 since the underestimation of the thermal capacitance in Eq.S12. Furthermore, without including the convection loss, the temperature will increase to about 12 K with the same modulation speed. The major discrepancy among the simulated temperature distribution shown in the inset of Fig. S4, our analytical calculation and our experimental results arises from excitation by a plane wave in simulation instead of a Gaussian beam.

REFERENCES

1. X. Liu, K. Fan, I. V. Shadrivov, and W. J. Padilla, "Experimental realization of a terahertz all-dielectric metasurface absorber," Opt. Express **25**, 191 (2017).
2. E. Snitzer, "Cylindrical Dielectric Waveguide Modes*," J. Opt. Soc. Am. **51**, 491 (1961).
3. L. R. Rayleigh, "XXXI. Investigations in optics, with special reference to the spectroscope," Philos. Mag. Ser. 5 **8**, 261–274 (1879).
4. H. Urey, "Spot size, depth-of-focus, and diffraction ring intensity formulas for truncated Gaussian beams," Appl. Opt. **43**, 620 (2004).
5. Y. Yang, A. Shutler, and D. Grischkowsky, "Measurement of the transmission of the atmosphere from 02 to 2 THz," Opt. Express **19**, 8830 (2011).
6. J. Johansson and N. Whyborn, "The diagonal horn as a submillimeter wave antenna," IEEE Trans. Microw. Theory Tech. **40**, 795–800 (1992).

7. S. Sommer, T. Raidt, B. M. Fischer, F. Katzenberg, J. C. Tiller, and M. Koch, "THz-Spectroscopy on High Density Polyethylene with Different Crystallinity," J. Infrared, Millimeter, Terahertz Waves **37**, 189–197 (2016).
8. T. L. Bergman and F. P. Incropera, *Fundamentals of heat and mass transfer.* (Wiley, 2011), 7th ed.